



Combining altimeter and subsurface float data to estimate the time-averaged circulation in the upper ocean

Josh K. Willis¹ and Lee-Lueng Fu¹

Received 12 December 2007; revised 22 August 2008; accepted 1 October 2008; published 17 December 2008.

[1] A new technique is presented for estimating time-averaged, upper ocean geostrophic velocity from a combination of altimeter data and subsurface float data. The technique makes use of the strong relationship between sea-surface height anomaly and anomalous velocity at depth to reduce mesoscale eddy variability in subsurface float displacements. The technique is demonstrated on a region in the North Atlantic that was well sampled by Argo floats. The 2004 through 2006 time-averaged density field was estimated from the surface to 2000 db by combining altimeter and hydrographic data from the floats. In addition, a reference velocity field was estimated at 1000 db based on a combination of altimeter data and subsurface float displacements. The reference velocity field was combined with geostrophic shear based on the density field to produce a three-dimensional estimate of geostrophic velocity from the surface to 2000 db. The Gulf Stream transport in the upper 2000 db is estimated to be 76 Sv at 73°W. In addition, an estimate of the 3-year average dynamic height at the surface was computed by combining the 1000-db reference dynamic height and the time-averaged density field.

Citation: Willis, J. K., and L.-L. Fu (2008), Combining altimeter and subsurface float data to estimate the time-averaged circulation in the upper ocean, *J. Geophys. Res.*, 113, C12017, doi:10.1029/2007JC004690.

1. Introduction

[2] Since 2000, the Argo project (<http://www.argo.net>) has sought to build a global ocean observing system based on subsurface floats that is capable of measuring the mid-depth circulation and stratification of the World Ocean. The floats provide estimates of subsurface velocity by drifting at a prescribed depth for a period of several days. The displacement between the float's final and initial positions provides an estimate of the time integrated velocity at depth.

[3] Having recently reached its goal of 3000 floats in the global ocean, the Argo array is now producing observations of the mid-depth circulation at an unprecedented rate. A number of previous studies have used subsurface float displacements to estimate the mid-depth circulation [Davis *et al.*, 1992; Davis, 1998, 2005; Lavender *et al.*, 2000, 2005]. In addition, Mercier *et al.* [1993] determined ocean circulation using hydrographic and float data in an inverse model; Rio and Hernandez [2004] used hydrographic, altimeter and surface drifter data to estimate the surface circulation. Nevertheless, the Argo and altimeter data provide complementary information about the circulation of the upper ocean and that has yet to be fully exploited.

[4] In particular, altimetric measurements of sea-surface height (SSH) anomalies provide information about ocean circulation on regional to global scales. Through the geostrophic relations, the spatial derivatives of SSH can be used

to infer geostrophic velocity at the ocean surface. Furthermore, velocity anomalies at the surface often penetrate to depths of 800 m or more [Roemmich and Gilson, 2001]. This suggests that altimeter data may be able to provide velocity information that is complementary to the Argo float displacement data.

[5] As noted by Davis *et al.* [1992], one of the largest sources of error in estimates of mean ocean circulation based on subsurface float displacements is caused by temporal variability related to the vigorous mesoscale eddy field. Because altimeter data provide information about anomalous geostrophic velocity, they may be used to remove some of the eddy variability from the subsurface displacement data. In this way, the complementary nature of the two observing systems is exploited to make improved estimates of the time-averaged circulation.

[6] In addition to the displacement data, Argo floats provide temperature and salinity profiles that can be used to infer velocity shear through the geostrophic relations. This allows us to vertically extend the velocity information provided by the float displacements to provide a full, three-dimensional estimate of the geostrophic circulation.

[7] Although both Argo and altimeter data now provide global coverage, the present analysis is performed using data from a somewhat limited region in order to make the problem more tractable. This allows for a more thorough comparison of the circulation estimate with previous results and for a more detailed description of the technique and its application. For these reasons, the present study was limited to data from the North Atlantic, north of 33°N. This region was chosen because of its global importance, as the circu-

¹Jet Propulsion Laboratory, Pasadena, California, USA.

lation in the far North Atlantic encompasses the source waters for the global thermohaline circulation. In addition, Argo data has been relatively abundant in the North Atlantic for some time. Finally, a number of previous estimates of subsurface circulation have been produced from independent subsurface float data [Lavender *et al.*, 2000, 2005] and will provide a basis of comparison and a means of evaluating the fidelity of the proposed technique.

[8] In the present study, the relationship between satellite altimeter measurements and subsurface float data is demonstrated, and a technique is presented for combining the two data sets to estimate the time-averaged (2004 to 2006), three-dimensional geostrophic velocity field for the N. Atlantic. The remainder of the article is organized as follows. Section 2 discusses the data sets used in the present estimate. Section 3 discusses how the Argo data are combined with SSH to estimate the time-averaged circulation. Results from the estimate of the upper ocean geostrophic velocity field are presented in section 4. Discussion and conclusions are given in section 5.

2. Data

2.1. Argo Data

[9] The goal of the Argo project has been to build and maintain a uniformly distributed, global array of 3000 autonomous floats that continuously monitor the circulation and properties of the world's oceans. Data from the Argo array of profiling floats were gathered from the U.S. Global Ocean Data Assimilation Experiment, Global Data Assembly Center (USGODAE GDAC) [<http://www.usgodaec.org/argo/argo.html>] and form the core of the present velocity analysis. The instruments that make up the array are isobaric profiling floats including APEX, SOLO and PROVOR floats. The floats operate by inflating a small, external rubber bladder to adjust their buoyancy and vertical position in the water column. The float's duty cycle begins by first diving to a specified depth and drifting with the ocean current for a period of several days. At the end of the drift period, the floats ascend and drift at the surface for a short time in order to fix their new position and transmit collected data via satellite. During either ascent or descent, the floats also dive beyond the drift depth, typically to a maximum depth of 2000 db, in order to produce a temperature and salinity profile.

2.1.1. Float Displacements

[10] Between the beginning of 2004 and the end of 2006, approximately 304 Argo floats were either deployed or drifted into the North Atlantic, north of 33°N. During this time, these instruments produced about 12,500 float displacements in this region, or about 360 float years of data.

[11] Displacements are computed by subtracting the position of a float at the end of its subsurface drift period from the position where it began its subsurface drift. This provides a time integrated estimate of velocity at the drift depth of the instrument. Unlike acoustically tracked floats, however, Argo float positions are determined using the ARGOS satellite network. Floats must therefore rise to the surface in order to determine their position. Several position fixes are usually obtained while the float drifts at the surface. However, floats often drift for a short period at the surface before satellite communication can be estab-

lished and again between the time of the last ARGOS position fix and the beginning of its next dive. This unmeasured drift introduces error into the subsurface displacements, and hence, the estimates of subsurface velocity. The final and initial subsurface positions of the floats must therefore be extrapolated using the positions and timing information measured during its drift at the surface.

[12] The technique suggested by Park *et al.* [2005] was used to extrapolate the unmeasured surface drift. This involves fitting a linear drift along with an inertial velocity to the surface position fixes. The resulting trajectory is used to extrapolate to the time at which the float surfaced (the "ascent end" time) and the time that it began its next dive (the "descent begin" time). Unfortunately, the "ascent end" and "descent begin" times are often inaccurate or go unreported by the float. Park *et al.* computed these times precisely using engineering data from the ARGOS transmissions. However, since the engineering data are not widely available to the public, the "ascent end" and "descent begin" times were approximated for floats that did not directly report them, such as SOLO-type instruments.

[13] Only about 25% of the displacements in the study region had usable "ascent end" or "descent begin" times. For the remaining 75%, these times had to be approximated. This was done by adding time to the first and last ARGOS position fixes for a given surface trajectory. The amount added was chosen so that the float's total time at the surface equaled the duration that the float was programmed to stay at the surface. If the float's programmed surface time was not reported, it was estimated by calculating the difference between the times of the first and last ARGOS position fixes for each cycle of a given float. The maximum value of this difference between the first and last fixes was then used as an estimate of the total time a float was programmed to stay at the surface.

[14] In cases where neither the "descent begin" nor the "ascent end" times were available, equal amounts of time were added to the times of the first and last position fixes. If only one was known, the excess time was added to the unknown end of the trajectory. These assumptions were tested using floats that contained valid "descent begin" and "ascent end" times and were found to give an RMS error of about 1 hour. This corresponds to a 1.8 km RMS error in displacement, averaged over the surface trajectories in the study region.

[15] Ascent and descent times range from 2 to 10 hours depending on the type of float and whether or not it measured a profile during transit. Using an estimate of geostrophic shear based on the density field described in section 3.1, position errors due to unmeasured drift during ascent and descent were estimated as described by Park *et al.* [2005]. Assuming a 10 hour ascent time, parking depth of 1000 m and profile depth of 2000 m, the median displacement error due to shear was 130 m, and 68% of errors were less than 180 m. These errors, combined with the errors due to unknown ascent and descent times, and the ~2 km error in the extrapolation technique reported by Park *et al.*, suggest an overall uncertainty of 2.7 km for displacements in the study region. For 10-day displacements, this corresponds to a 0.3 cm/s uncertainty in the subsurface velocity estimates. As shown below, this error is much

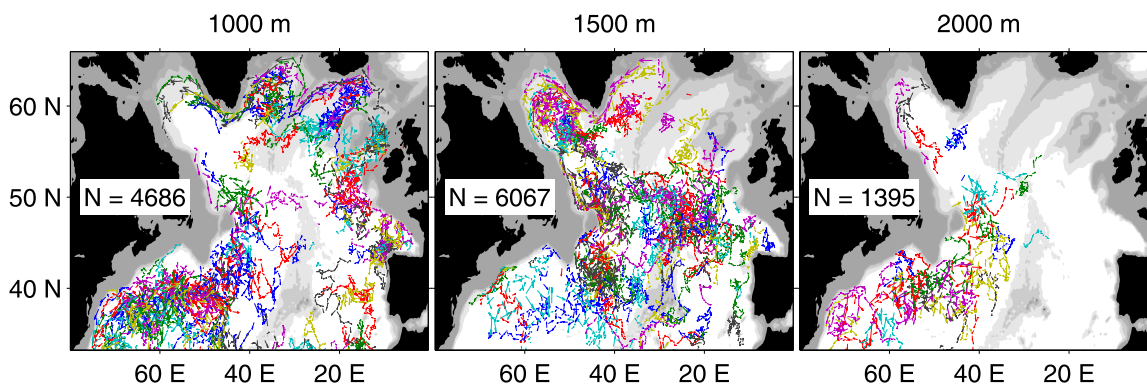


Figure 1. Float displacements by parking depth. All displacements for a given float have the same color. From light to dark, shading indicates bathymetry <4000 m, <3000 m, <2000 m, <1000 m, and <500 m.

smaller than sampling errors related to unresolved meso-scale variability.

[16] Although the recommended parking depth for Argo floats is 1000 m, only about 36% of float displacement data available in the study region actually parked at depths within 100 m of this depth. About 50% parked at depths close to 1500 m and 11% parked close to 2000 m, with the remainder parking at intermediate depths. Figure 1 shows float displacements at the three different depths, with data from each float represented by a single color.

2.1.2. Profile Data

[17] In situ temperature and salinity profiles from Argo floats were used to estimate the density field. All of the profile data containing pressure errors as discussed by Willis *et al.* [2007, 2008] have now been corrected or flagged as discussed on the Argo Web site (http://www-argo.ucsd.edu/Acpres_offset2.html). These profiles were therefore included in the present analysis provided they were flagged as “good” in the metadata. Delayed-mode data were used where available, and Argo quality control flags were used to eliminate spurious measurements. Additional quality control was performed in two steps. First, all data were grouped together in 10° latitude bands and visually inspected to remove gross outliers. Profiles were then divided into $5^\circ \times 5^\circ$ horizontal boxes and a standard deviation check was performed in each box. Profiles were compared with temperature and salinity from the WOCE gridded hydrographic climatology [Gouretski and Koltermann, 2004, hereafter WGHC] and profiles with data more than three standard deviations away were removed. The profiles were then linearly interpolated onto a uniform 10 db grid for analysis. This yielded about 12,000 usable temperature and salinity profiles in the study region.

[18] Density anomalies relative to the WGHC were used to compute density maps and for comparison with altimeter data. Although the majority of floats obtained temperature and salinity measurements to a depth of 2000 db, about 10% of floats were missing data below 1000 db, and another 10% were missing data below 1500 db. Density anomaly profiles for these data were “extended” to 2000 m using the technique suggested by Smeed and Alderson [1997]. Errors in this technique were tested using complete profiles in the region and found to give RMS errors in dynamic height of only 1.1 cm and 0.6 cm, profiles with no data below 1000 m and 1500 m respectively. As discussed below, these errors

are small compared with the sampling errors caused by unresolved mesoscale variability.

2.2. Altimeter Data

[19] Gridded, sea-surface height anomaly fields containing data from multiple satellite altimeters were obtained from AVISO (<http://www.aviso.oceanobs.com>). The delayed mode product, DT-MSLA “Upd” was used for the period of the study. These data are provided on a $1/3^\circ \times 1/3^\circ$ Mercator grid, with one map every 7 days.

[20] The AVISO data are supplied as anomalies relative to a seven-year mean of the sea-surface height field. The goal of the present analysis is to determine the mean geostrophic circulation in the N. Atlantic for the period from the beginning 2004 through the end 2006. For consistency, the time-average over this period was removed from the AVISO data prior to the analysis.

3. Combining Altimeter and Float Data

3.1. Density

[21] In order to fully exploit the velocity information contained in the altimeter and Argo data, it is necessary to first estimate geostrophic shear using the Argo profile data. This is used to combine float displacement data from different depths as well as to estimate the three-dimensional, time-averaged geostrophic velocity field. An estimate of the time-averaged density field is therefore computed first.

[22] A number of previous studies [Gilson *et al.*, 1998; Willis *et al.*, 2004] have shown that sea-surface height variability is strongly correlated with changes in upper ocean density. Furthermore, Willis *et al.* [2003] showed that combining altimeter and profile data can provide estimates of upper ocean density variability with less error than either data set individually.

[23] In the present analysis, a technique similar to the one used by Willis *et al.* [2003] is used to reduce the sampling error caused by the mesoscale eddy field. The eddy variability in the density field is estimated using the AVISO SSH anomaly maps and linear regression coefficients of SSH onto density anomaly as a function of position and depth.

[24] The spatially varying mean over the period of interest (January 2004 through December 2006) is first removed from the SSH fields. Regression coefficients $\alpha(x, y, z)$ of SSH anomaly onto density anomaly were then

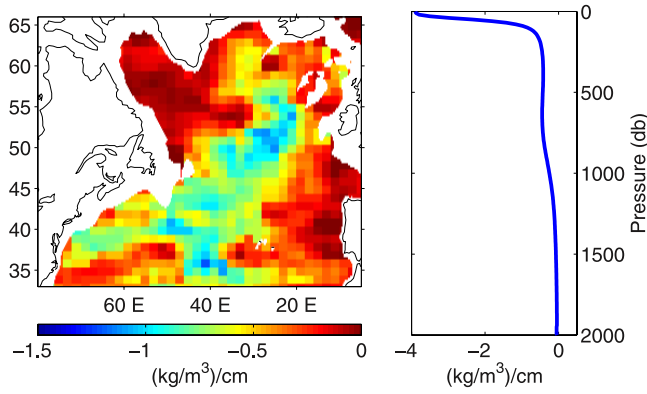


Figure 2. (left) Linear regression coefficient of SSH onto 500 m density anomaly. (right) Regression coefficient versus depth, averaged over the study region.

computed in 4° longitude by 2° latitude by 10 db pressure bins from the surface to 2000 db using density anomaly profiles and SSH interpolated to the time and location of each profile. Figure 2 shows the spatial distribution of the regression coefficients as well as the depth dependence of their basin average.

[25] In the notation of *Willis et al.* [2004], the estimate of time-averaged density is computed as:

$$\rho_{\text{estimate}} = \left\{ \rho_{\text{profile}} - \alpha \times \text{SSH} \right\} + \overline{\alpha \times \text{SSH}} \quad (1)$$

[26] Here, the curly brackets represent objective mapping [Bretherton *et al.*, 1976] and the over bar represents the time average over the study period. The last term in (1) equals zero by design, as the time average of the SSH maps over the study period was removed at the outset. Equation (1) therefore reduces to an objective map of the density anomaly profiles with some of the temporal variability removed using the regression coefficients and altimeter data. This is similar to the “combined estimate” approach used by *Rio and Hernandez* [2004] to estimate the mean dynamic topography using altimeter and in situ data.

[27] Subtraction of $\alpha \times \text{SSH}$ significantly reduces the variance of the density anomaly data in the study region. To test this, profile data were divided into independent sets, before and after 1 July 2004. The latter set were used to determine α , and the former set were used to test the effect of subtracting $\alpha \times \text{SSH}$ from the density anomaly data. Although only half of the data were used to compute α for this experiment, there were no significant differences between this estimate of α and the ones computed using all of the data. Using data beyond the 2004 through 2006 period of the time average, this included about 17,500 profiles after to 1 July 2004 and about 9600 profiles before. Figure 3 shows the RMS variability of density anomaly versus depth, with and without subtraction of $\alpha \times \text{SSH}$. The ratio of the variance is also shown. On average, the variance is reduced by about 32%. Although the variance is reduced at all depths, the largest reduction occurs around the depth of the thermocline. This improves signal to noise ratio and suggests that when the altimeter data are used, fewer observations are required to produce a stable estimate of time-averaged density for the study period.

[28] Prior to computing the objective maps, density anomaly data were averaged in $1/4^\circ \times 1/4^\circ$ bins. The geographic center of the profiles in each bin was computed and used along with the bin averages as input data for the objective map. This reduced the number of observations used in the objective map to about 8100, making it computationally feasible on a modern workstation.

[29] The covariance function used for the objective map of density was similar to the two-scale function suggested by *Willis et al.* [2004]. However, the large-scale exponential term was replaced with a Gaussian term and the small-scale Gaussian term was replaced with the covariance function used by *Rio and Hernandez* [2004]:

$$\langle \rho_i \rho_j \rangle = \left[\frac{1}{2} (1 + r + \frac{1}{6} r^2 - \frac{1}{6} r^3) \exp(-r) + \frac{1}{2} \exp(-R^2) \right] + n \delta_{ij}, \quad (2)$$

where

$$r = \text{sqrt} \left[(x_i - x_j)^2 / l_x^2 + (y_i - y_j)^2 / l_y^2 \right],$$

$$R = \text{sqrt} \left[(x_i - x_j)^2 / L_x^2 + (y_i - y_j)^2 / L_y^2 \right].$$

Here, (x, y) are the positions of the bin-averages, l_x and l_y are zonal and meridional scales of the short-scale part of the covariance function, and L_x and L_y are zonal and meridional scales of the large-scale part. The noise to signal ratio, n , represents temporal variability as well as sub-mesoscale variations and instrument noise that will be excluded from the mapped fields. This form was found to fit the observed data covariance extremely well (Figure 4).

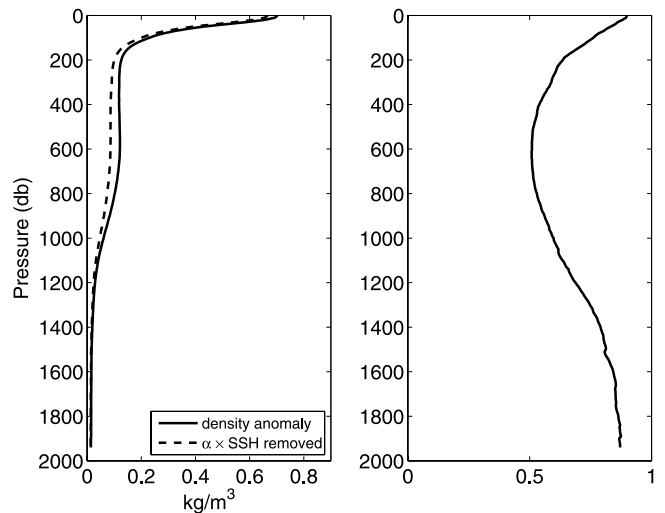


Figure 3. (left) RMS variability of density anomaly versus depth before and after subtraction of $\alpha \times \text{SSH}$. (right) The right panel shows the ratio of variance before and after subtraction of $\alpha \times \text{SSH}$. For the purposes of this calculation, data were divided into two independent sets as described in the text. Regression coefficients calculated using one set were used to test variance reduction in the other.

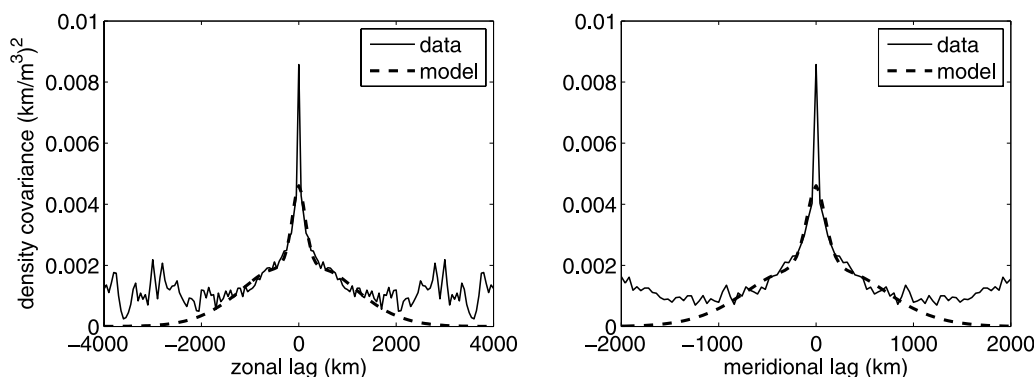


Figure 4. (left) Zonal and (right) meridional depth-averaged density covariance. Solid lines are computed from bin-averaged density data and dashed lines show model covariance.

[30] To determine the appropriate choices for the noise to signal ratio and the zonal and meridional covariance scales, the depth-averaged covariance for density anomaly function was estimated from the $1/4^\circ$ data. A nonlinear fit of (2) to the estimated covariance gave zonal and meridional scales of $L_x = 1330$ km, and $L_y = 763$ km for the large-scale term, and $l_x = 76.7$ km, and $l_y = 52.9$ km for the small-scale term. The zero-lag bin was not included as part of the fit and the noise to signal ratio was estimated as the ratio of variances above and below the peak of the resulting covariance function at the zero lag. A noise to signal ratio of 0.96 was found to be appropriate for the covariance of the raw data, and 0.86 for the SSH-corrected data. The smaller noise variance of the SSH-corrected density anomalies reflects the reduced mesoscale and temporal variability, as expected from Figure 3. The noise to signal ratio does not reflect all of the 24% variance reduction because there is also a reduction in covariance at non-zero lags when the scaled altimeter data is subtracted. This is expected, as the temporal variability in both SSH and subsurface density also contains variance on a wide range of length scales. For consistency, the same covariance scales were used at all

depths. Although this restriction is not theoretically necessary, previous work has suggested that the shape of the wave number spectrum is relatively depth independent for variability in the upper 800 m of the ocean [Zang and Wunsch, 2001]. Furthermore, the a posteriori test of the covariance function described below suggests that the lack of depth dependence was not problematic.

[31] The bin-averaged density data were objectively mapped onto a $1/4^\circ \times 1/4^\circ \times 10$ db grid. Figure 5 shows the 2004 through 2006, time-averaged density fields at the surface, 500 db, 1000 db, and 1500 db. The sharp gradient across the western boundary current as well as the subpolar gyre boundaries are clearly visible for all depths except the surface. In addition, the Mann eddy [Mann, 1967] is visible as a low-density bulls-eye at just offshore of the North Atlantic Current at 42°N . Figure 6 shows the map of skill associated with the density maps, where skill is defined as one minus the ratio of the estimated error variance to the expected signal variance. A skill of 0.7 (0.9) implies an RMS error of 0.3 (0.2) kg m^{-3} at the surface, 0.06 (0.03) kg m^{-3} at 500 db, 0.03 (0.02) kg m^{-3} at 1000 db, and 0.01 (0.005) kg m^{-3} at 1500 db.

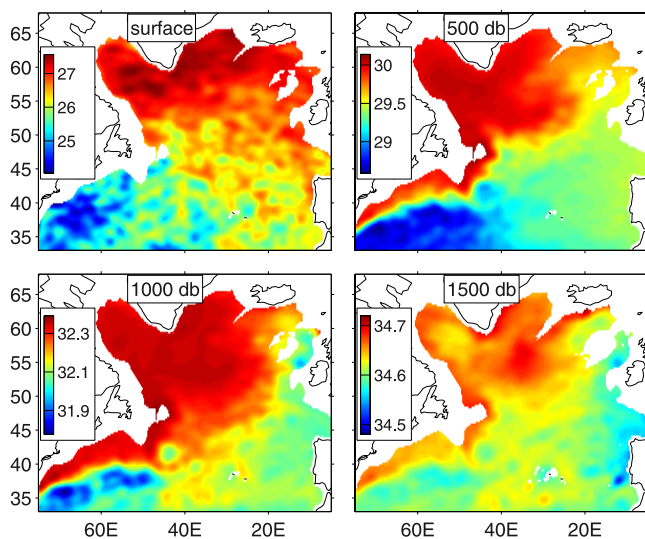


Figure 5. (upper left) Time averaged density field at the surface, (upper right) 500 db, (lower left) 1000 db, and (lower right) 1500 db.

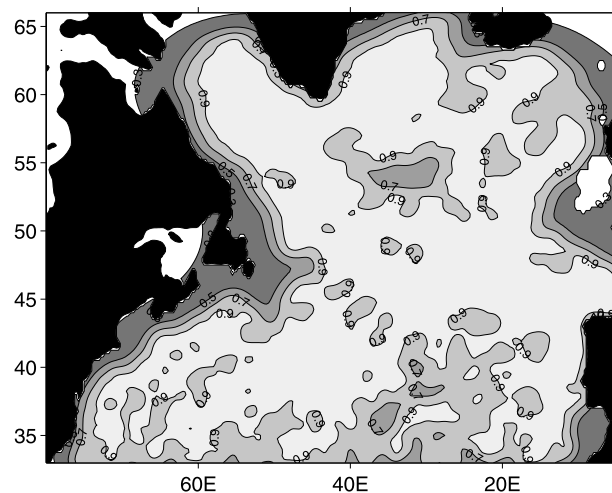


Figure 6. Skill in the density field. Contours go from 0.3 to 0.9 with a spacing of 0.2. The median skill value in the study region was 0.90.

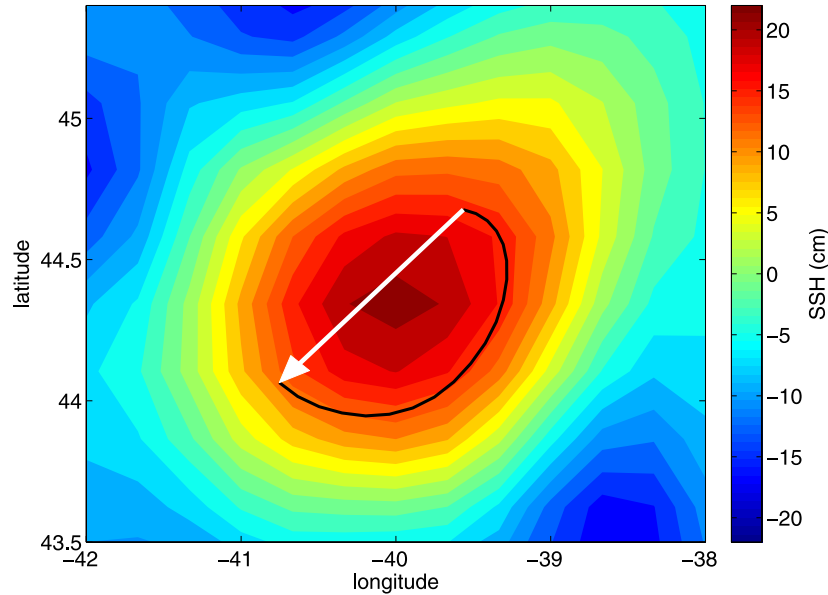


Figure 7. A pseudo-displacement (white arrow) computed by advecting an imaginary particle through the geostrophic velocity field implied by SSH for the duration of subsurface drift of an Argo float. Background field is SSH. Contour interval is 2 cm.

[32] Because the skill map and error estimates are somewhat sensitive to the choice of covariance function, an a posteriori test of the statistical assumptions was performed by comparing the mapped product with the original density data. The covariance field was recomputed after subtracting the mapped density field from the density data. The resulting covariance function had no significant structure at any depth and the noise variance was comparable to the noise to signal ratio used in the objective map. This suggests that the choice of length scales and noise to signal ratios was justified and that the lack of depth dependence in the covariance function did not significantly impact the estimate.

3.2. Absolute Subsurface Velocity

3.2.1. Combining Float Displacements With Altimeter Data

[33] The horizontal gradients of density can be used to determine geostrophic velocity based on the thermal wind equations. Such estimates, however, have always suffered from lack of knowledge of the two-dimensional reference velocity field. Subsurface float displacements from the Argo array now provide direct observations of the reference velocity at depth. Nevertheless, significant temporal averaging is required in order to estimate the time-averaged circulation because of the vigorous mesoscale eddy field. As with the density data, it is possible to reduce the effects of the mesoscale variability using SSH data. The approach adopted here is similar to that of *Niiler et al.* [2003] who used altimeter data to reduce temporal variability in surface drifter data.

[34] In order to reduce eddy-variability in the subsurface float displacement data, anomalous geostrophic velocity at the surface is calculated from SSH anomaly using the geostrophic relation:

$$fu = -g \frac{\partial \eta}{\partial y}, \quad -fv = -g \frac{\partial \eta}{\partial x}, \quad (3)$$

where $\eta(x, y, t)$ is SSH anomaly and f is the Coriolis parameter that varies with latitude. For each float displacement, the anomalous geostrophic surface velocities, u and v , are linearly interpolated to the time and location of the beginning subsurface position. A trajectory is then computed by integrating the velocities forward in time by an amount equal to the float's subsurface drift period. The vector displacement from the beginning to end of the virtual trajectory is referred to as the "pseudodisplacement" (Figure 7).

[35] *Roemmich and Gilson* [2001] showed that dynamic height and geostrophic velocity anomalies associated with eddies in the subtropical North Pacific extended from the surface to a depth of at least 800 m, decreasing in amplitude and tilting slightly eastward with depth. This suggests that anomalous geostrophic surface velocities observed by the altimeter may have a subsurface signature as well. Numerous other studies [*Gilson et al.*, 1998; *Wilson et al.*, 2002; *Guinehut et al.*, 2006, etc.] have also demonstrated a relationship between altimeter data and subsurface velocities. To test for such a relationship in the present data, pseudodisplacements were compared with observed 1000 db displacements for the region from 50°W to 40°W, 33°N to 36°N (Figure 8). A clear correlation exists between the pseudodisplacements and the observed displacements, with the pseudodisplacements consistently overestimating the observed displacements.

[36] A linear regression of observed displacements onto pseudodisplacements was computed. For the data shown in Figure 8, the regression coefficients were found to be $0.23 \pm .05$ in the zonal direction and 0.22 ± 0.05 in the meridional direction, where error bars represent the 95% confidence interval. No significant differences were found between meridional and zonal regression coefficients in the study region. This suggests that the regression coefficients used to project SSH anomalies onto the subsurface displacements can be simplified to a single factor, β ,

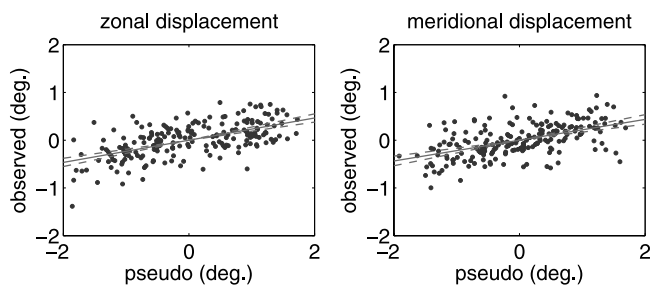


Figure 8. Comparison of observed displacements and pseudo-displacements from 184 Argo floats drifting at 1000 db between 50°W to 40°W, 33°N to 36°N (dots). Solid line shows regression coefficient, dashed lines show 95% confidence interval for regression coefficient.

which multiplies η in equation (3). Although more sophisticated treatments may be possible that account for features such as the eddy tilt observed by *Roemmich and Gilson* [2001], this choice still allows for significant reduction of eddy variability in the displacement data.

[37] The regression coefficients, β , that project SSH anomaly onto subsurface displacements were computed in 10° longitude by 3° latitude bins and separately for data from each of the three drift depths (Figure 9). Although bins of this size were necessary in order to achieve sufficient data density, the regression coefficients were computed on a 2° longitude by 1° latitude grid using overlapping bins. A mean velocity was computed for each bin and removed from the observed displacements prior to computing the coefficients. As no significant differences were found between meridional and zonal coefficients, the meridional and zonal

components of each displacement and pseudodisplacement were treated as independent observations in the calculation of the regression coefficient.

[38] Also shown in Figure 9 are the correlation coefficients, r , between observed and pseudo displacements each of the three depths. At 1000 m, the correlation between SSH and subsurface velocity are greater than 0.5 in most regions. At 1500 and 2000 m, the correlations are smaller but remain above 0.3 in most regions. In the Labrador Sea, west of the southern tip of Greenland, high correlations are observed in both the 1500 m and 2000 m velocity data. The significant correlation between SSH and velocities at depths of 1000 m and greater suggests that either deep baroclinic or barotropic variability is significant in the North Atlantic. This region also contains vigorous eddies that extend deep into the weakly stratified water column of the Labrador Sea [*Lilly et al.*, 2003]. This is consistent with the results of *Guinehut et al.* [2006] who found that SSH variations in the North Atlantic could not be fully explained by baroclinic variability in the upper 700 m or by Sverdrup transport.

[39] Once computed, the regression coefficients and SSH data were used to reduce eddy variability in the float displacement data. An adjusted pseudodisplacement was computed by interpolating the regression coefficient for the appropriate drift depth to the location of each observed displacement. The regression coefficient, β , was then multiplied by η in equation (3), which was integrated over the subsurface drift period. The resulting adjusted pseudodisplacement was then subtracted from the observed displacement. This reduces the basin-average variability of subsurface velocities from displacement data from 7.8 cm/s to 6.7 cm/s.

[40] To further illustrate the reduction in eddy variability, bin averages of meridional and zonal velocity were esti-

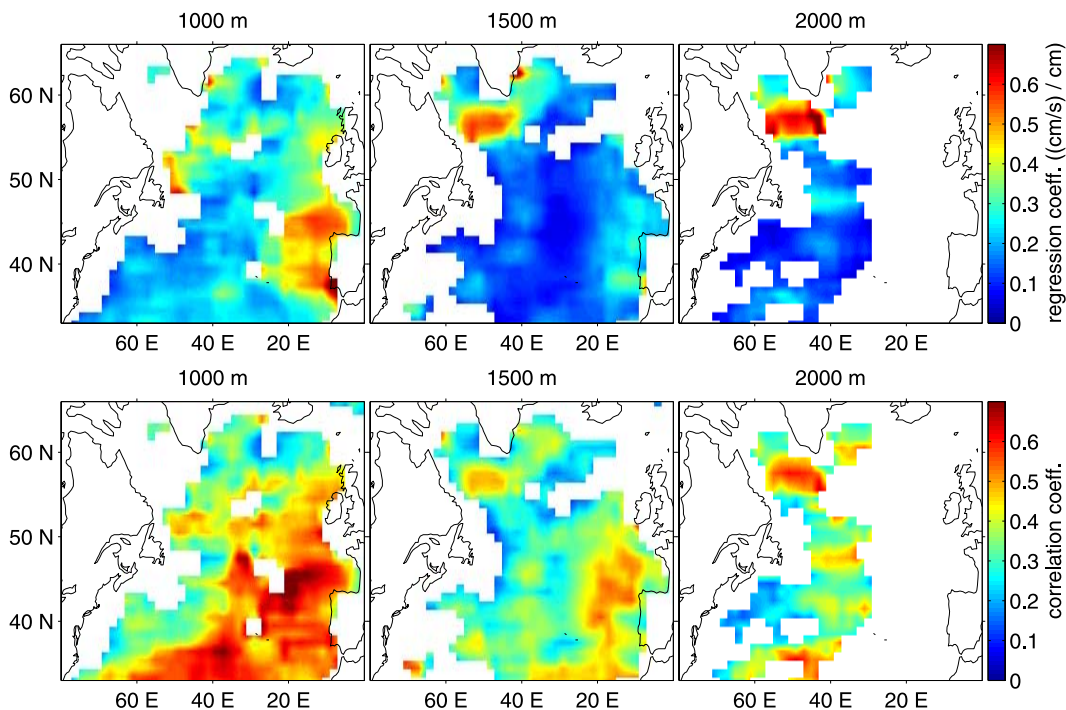


Figure 9. Coefficient of regression (top row) of pseudo-displacements onto observed displacements for each of the three drift depths. Also shown are the correlation coefficients, r , for each depth (bottom row). Only regions with correlations significant at the 95% level are plotted.

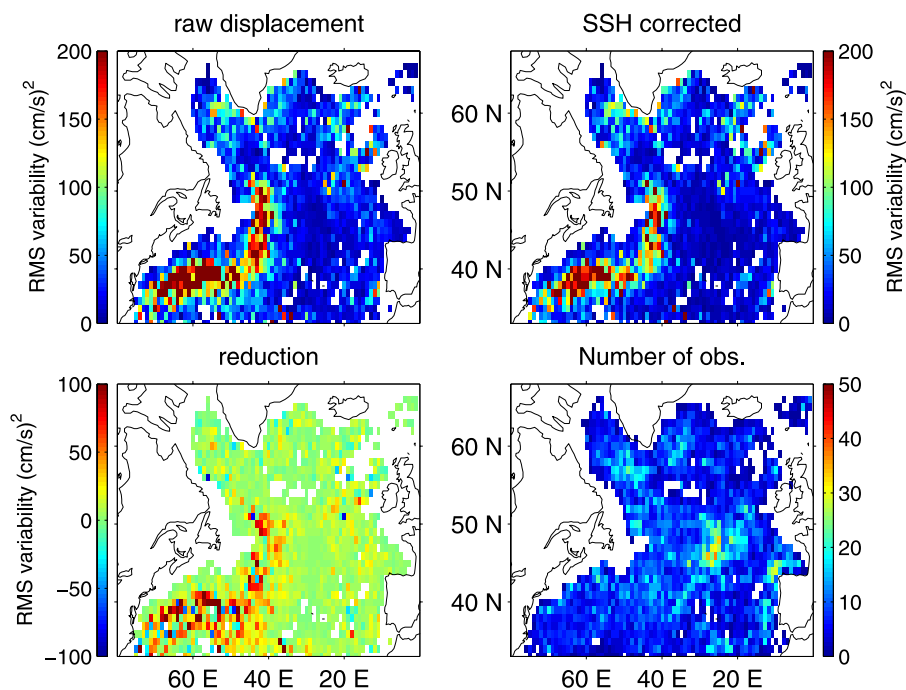


Figure 10. Variability of subsurface displacements in one-degree squares (top left) before and (top right) after subtraction of adjusted, pseudo-displacements. The lower left panel shows the difference between the two upper panels and the lower right shows the number of observations in each one-degree square. For the purposes of this calculation, data were divided into two independent sets as described in the text. Regression coefficients calculated using one set were used to test variance reduction in the other.

mated from the displacements on a 1° grid (Figure 10). Although a finer grid was used to make objective maps as described below, the 1° grid allows for sufficient observations in most bins to produce a stable, long-term average. Eddy variability is estimated relative to the 1° means. Again, data were divided into independent sets to test the effect of variance reduction. However, because coverage at different drift depths changed significantly over the study period, this was accomplished by placing every other displacement from a given float into opposite sets. One set was used to determine the coefficients β and the other was used to test the effects of variance reduction. Almost all regions have reduced variability after subtracting the adjusted pseudodisplacements and the median reduction in variance was 24%. This represents a 24% reduction in the noise-to-signal ratio for estimating the time-averaged velocity.

3.2.2. Objective Mapping

[41] Techniques for analysis of subsurface float displacement data have been developed and applied in several previous studies, including those of *Davis* [1998, 2005] and *Lavender et al.* [2000, 2005]. In the present study, we use the technique developed by *Davis* [1998] to objectively map geostrophic pressure and velocity from the SSH-corrected float displacements.

[42] Observations from the three different drift depths were combined to estimate the time-averaged velocity at 1000 db. To do so, geostrophic shear was calculated from the time-averaged density field (Figure 5) using the thermal wind equations and adjustments were made to the 1500 db and 2000 db float displacements.

[43] As in the study of *Davis* [1998], weighted, space-time averages of displacement data were used as input to the objective map. The space-time averages were initially computed on a $1/4^\circ \times 1/4^\circ$ grid but were re-centered to the position-weighted average of the data for each grid point. Also, as recommended by *Davis et al.* [1992], all averages were computed by weighting the measurements by the duration that the float was submerged to produce unbiased estimates. Although a number of Argo floats are programmed to have different subsurface drift periods, the majority (about 78%) drift for 10 days, so these averages differ only slightly from simple averages.

[44] The covariance function for geostrophic pressure was chosen to have a similar functional form as the covariance function for the density maps. However, a dependence on barotropic potential vorticity was also included as recommended by *Lavender et al.* [2005]. This gives the following functional form:

$$\langle p_i p_j \rangle = [1/2(1 + r + 1/6r^2 - 1/6r^3) \exp(-r) + 1/2 \exp(-R^2)] \cdot \exp(-\Omega) + n \delta_{ij}, \quad (4)$$

for geostrophic pressure covariance, where $\Omega = (\zeta_i - \zeta_j)^2 / (\zeta_i^2 + \zeta_j^2)$. Here ζ is barotropic potential vorticity, or f/H , where f is the Coriolis parameter and H is the water depth.

[45] *Davis* [1998] and *Lavender* [2001] showed that the covariance functions needed to map geostrophic pressure and velocity from displacement data can be derived from the geostrophic relation and they are proportional to the

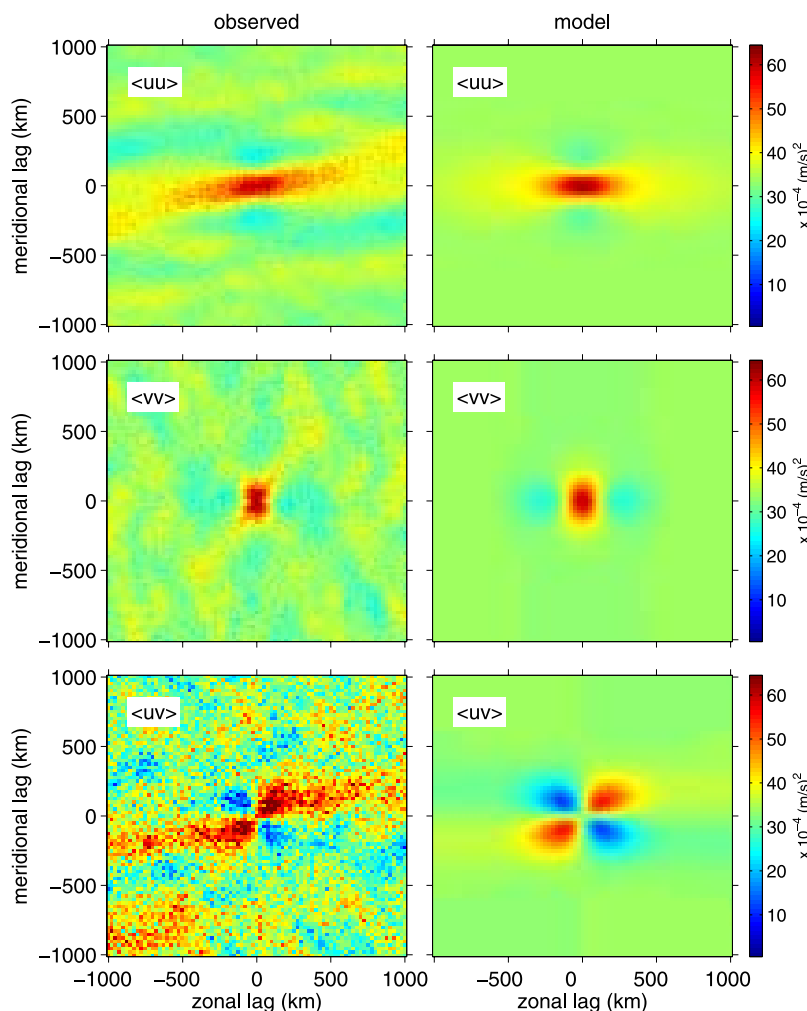


Figure 11. Observed and model covariance functions for displacement data versus zonal and meridional lag.

spatial derivatives of the covariance function for geostrophic pressure. Estimates of the 2-D spatial-lag covariance functions $\langle uu \rangle$, $\langle vv \rangle$, and $\langle uv \rangle$ were computed from the $1/4^\circ$ bin-averaged velocities and a nonlinear fit was used to determine the length scales. Zonal and meridional covariance scales were estimated to be $L_x = 983$ km, and $L_y = 273$ km for the large-scale term, and $l_x = 111$ km, and $l_y = 83.4$ km for the small-scale term. Figure 11 shows that the observed covariance functions are in excellent agreement with those derived from (4). As for density, the noise to signal ratio was determined by comparing the covariance function at zero lag with the data variance. A noise to signal ratio of 2.8 was found to be appropriate for the covariance of the raw data, and 3.0 for the SSH-corrected data. Again, both the amplitude of the covariance function and the noise variance were significantly reduced by the SSH-correction. However, for the displacement data, the reduction in signal variance was slightly larger than the reduction of noise variance. This is the reason for the slight increase in the noise ratio of the SSH-corrected data.

[46] After applying the geostrophic shear adjustment to the deep displacements, reducing the eddy variability and averaging in $1/4^\circ$ bins, objective maps [Bretherton *et al.*, 1976] of

the time-averaged velocity and geostrophic pressure at 1000 db were computed (Figure 12). To the south of the Gulf Stream, the tight recirculation gyre is clearly visible. As in the density fields, the Mann eddy is also well-resolved in the three-year average velocity estimate. In the northern part of the domain, the deep subpolar gyre is denoted by blue and purple regions in the contour map of dynamic height. In addition, the recirculation gyres along the northern and western boundary of the subpolar gyre first described by Lavender *et al.* [2000] are visible within the purple contours.

[47] Figure 13 shows the skill map associated with the 1000 db dynamic pressure and velocity maps. A skill of 0.7 (0.9) results corresponds to an RMS error of 1.9 (1.1) cm in dynamic pressure or 3.8 (2.2) cm/s in velocity.

[48] At the suggestion of one reviewer, an additional calculation was carried out to verify that the errors suggested by Figure 13 are reasonable. Two independent estimates of 1000 db dynamic pressure were computed by randomly splitting the 12,500 displacement observations into two independent groups. Comparing these two independent estimates with each other provides an independent assessment of the errors in the estimate as well as a means

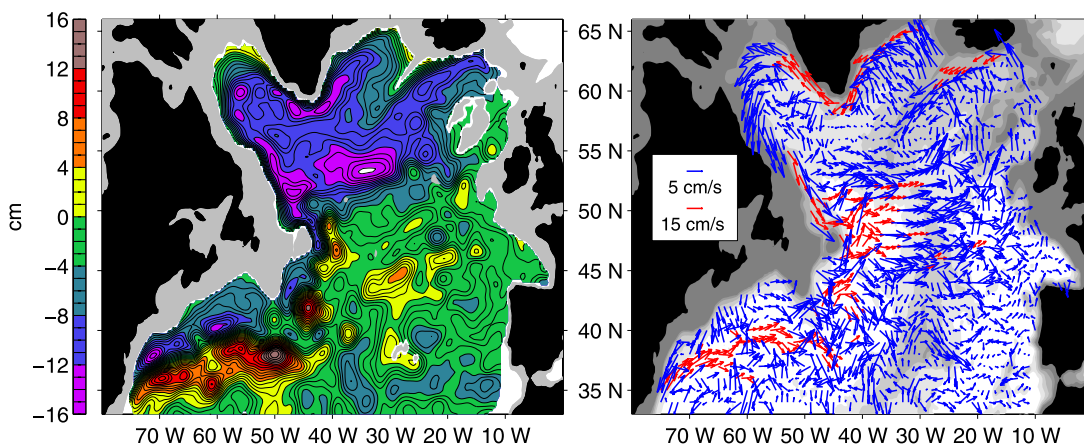


Figure 12. Time-averaged circulation at 1000 db mapped from SSH-corrected float displacements. Left panel shows dynamic height in cm (contour interval is 1 cm). Right panel shows the corresponding velocity field. Regions with skill less than 0.6 are not plotted. Note that red vectors are plotted at 1/3 the scale of the blue vectors. Bathymetry is shaded as indicated in Figure 1.

of verifying the error estimates computed using the objective mapping technique.

[49] The difference between the two independent estimates is shown in Figure 14, along with its probability distribution function (PDF). In the regions with skill greater than 0.05, the RMS difference between the two independent estimates was 1.7 cm. This is in excellent agreement with the RMS error predicted by the skill maps of the two estimates.

[50] To test how well the error computed using the objective mapping technique predicts the differences shown in Figure 14, an error estimate was made by averaging the skill maps from the two independent estimates together and scaling them as follows: $error = \sqrt{A * (1 - sk)}$, where A is the signal variance used in the mapping procedure and sk is the average skill map. The difference between the two estimates of dynamic height was then normalized using this error map. The PDF of the normalized error is very close to the standard normal distribution, with approximately 69% of the two independent estimates falling within one standard

error of each other as predicted by the objective mapping error. This suggests that the error estimates based on Figure 13 are realistic and that the objective mapping procedure returns realistic error estimates when appropriate statistical assumptions are made.

4. Results

[51] The thermal wind equations were used to estimate geostrophic shear from the density maps described in section 2. Using the 1000 db maps of velocity as a

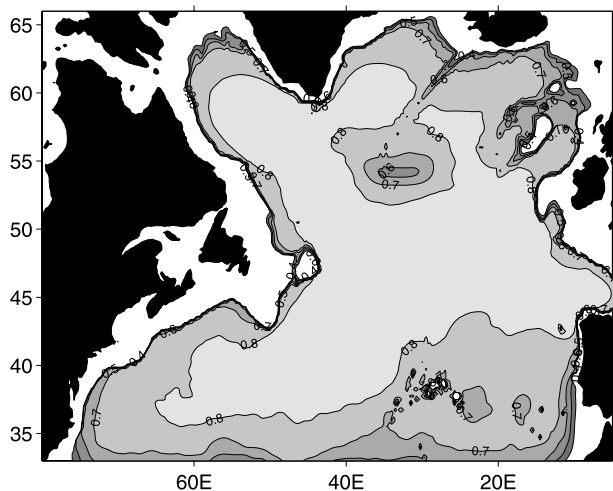


Figure 13. Skill map of 1000 db circulation. Contours go from 0.4 to 0.9 with a spacing of 0.1. The median skill value in the study region was 0.80.

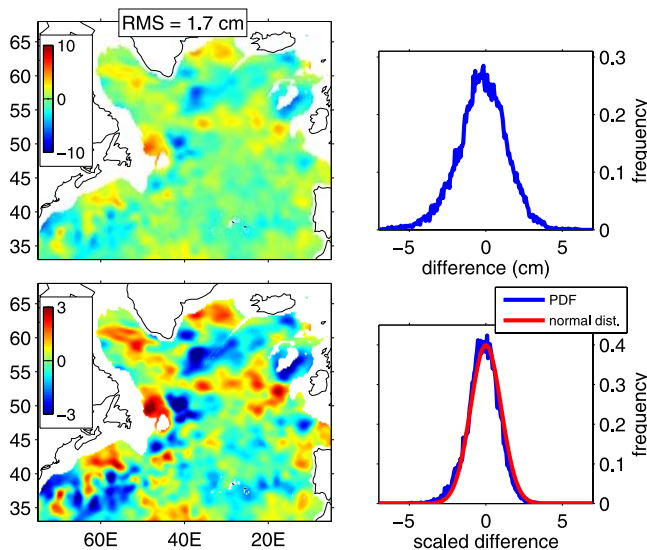


Figure 14. Difference between estimates of 1000 db dynamic height made from 2 independent sets of displacement data (upper-left panel). The RMS difference is 1.7 cm. The upper-right panel shows the probability distribution function (PDF) of the differences from the upper-left panel. The lower-left panel also shows the difference, but divided by the error predicted from the objective map. The lower-right panel shows the PDF of the scaled differences (blue) along with the standard normal distribution with zero mean and unit variance (red).

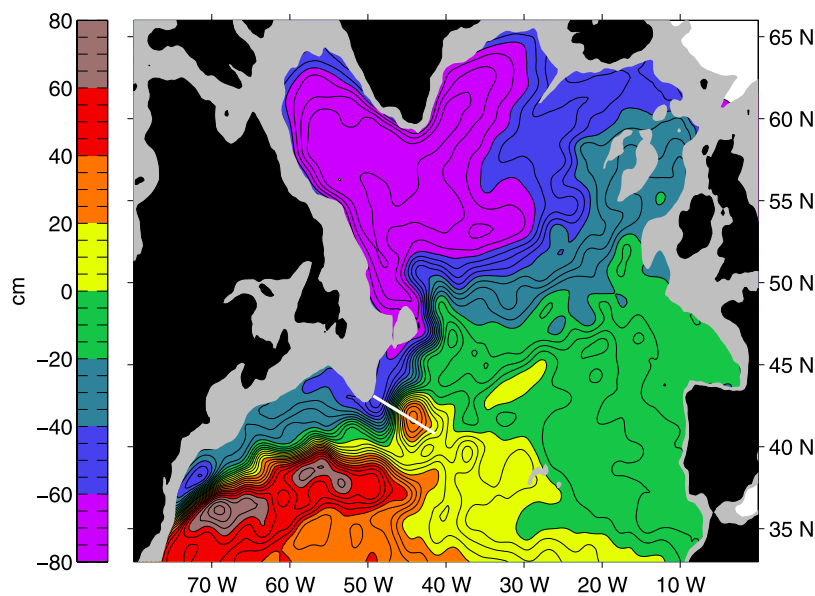


Figure 15. Surface dynamic height averaged over the period from 2004 through 2006. The contour interval is 5 cm. Map is limited to regions of skill greater than 0.6 and by the 1000 m isobath as discussed in the text. The white line shows the ‘virtual transect’ along which velocity is plotted in Figure 15.

reference, a three-dimensional estimate of the circulation was constructed. This estimate represents the three-year time average of the geostrophic, horizontal circulation in the North Atlantic from the surface to 2000 db.

[52] In addition to velocity, steric height from the surface relative to 1000 db was computed. By adding this to the 1000 db dynamic height from section 3.2, a time-averaged estimate of surface dynamic height was constructed (Figure 15). Because the 1000 db dynamic height is used as a reference, the estimate of surface dynamic height is limited in extent by the 1000 m isobath.

[53] The surface expression of the subpolar gyre is visible in the purple shaded contours in Figure 15. In addition, the Azores current is just visible at the southern edge of the study region as an eastward flowing current centered at 34°N and beginning at about 45°W.

[54] Figure 16 shows a velocity section across the Gulf Stream at the location illustrated by the white line in Figure 15. This is the same section occupied by *Meinen* [2001]. At the surface, the peak velocity of the current is 40 ± 2 cm/s, and the difference in dynamic height across the Gulf Stream is 95 ± 3 cm. This is significantly slower than the peak surface velocity estimated by *Meinen* of about 60 cm/s for the Eulerian average at this section (see *Meinen*’s, Figure 8).

[55] This discrepancy between the peak surface velocities is caused by a slowing of the Mann Eddy [*Mann*, 1967] between the mid-1990s and the mid-2000s. Figure 17 shows sea-surface height and surface geostrophic velocity averaged over the period of the present study (2004 through 2006) and the period of the study of *Meinen* [2001] (August 1993 through February 1995). This was computed by combining the mean SSH estimate shown in Figure 16 with the 14-year record of SSH variability from AVISO. The more vigorous Mann Eddy is clear from both the higher peak in SSH as well as the more positive and negative lobes in surface velocity for the earlier period. The 60 cm/s peak

velocity for the earlier period in Figure 17 is in excellent agreement with that of *Meinen* [2001].

[56] The total transport of the current in the upper 2000 m was 70 Sv for the section shown in Figure 16. *Meinen* [2001] reported a baroclinic transport for the upper 2000 m of the North Atlantic Current of 57 Sv across this section. Assuming an average bottom depth of 4300 m and *Meinen*’s [2001] estimate of barotropic transport, the total transport of the North Atlantic Current would be about 74 Sv for the upper 2000 m for the period 1993–95. This is slightly higher than the 70 Sv estimate for our 2004–06 estimate, but well within *Meinen*’s 14 Sv error bounds. It may also reflect interannual variability in the transport.

[57] At 73°W, *Halkin and Rossby* [1985] estimated the mean transport of upper 2000 m the Gulf Stream to be 88 Sv. Along the same section in the present estimate (not shown), we estimate the transport to be 76 Sv. This is

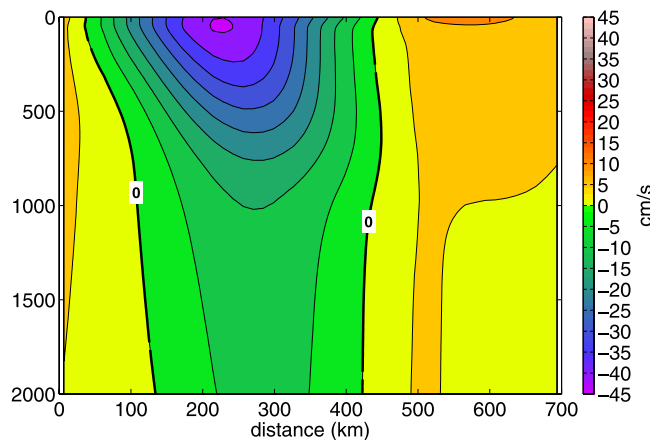


Figure 16. Velocity versus pressure and distance along the transect shown in Figure 14. North is to the left and negative velocities (into the page) represent flow to the northeast.

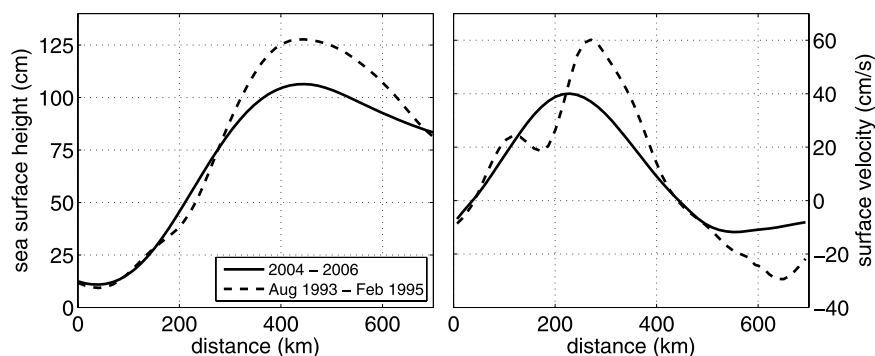


Figure 17. (left) Time-averaged SSH and (right) surface velocity along the section studied by *Meinen* [2001] for the period of the present study (solid line) and the period of the data used by *Meinen* [2001] (dashed line). Note the Mann Eddy, centred at 450 km, is more vigorous in the earlier period. The temporal record of SSH was constructed by combining the mean SSH estimates from Figure 12 with the AVISO record of SSH variability.

somewhat lower than the mean value reported by Halkin and Rossby, but it is not outside the range of transports estimated from individual transects. Nevertheless, the present study also encompasses a period of slowing for the Gulf Stream at 73°W . This is illustrated by a time series of the difference between the maximum and minimum SSH along this section (Figure 18) computed from the AVISO record of SSH variability and mean SSH from the present study. The steady decrease beginning in early 2004 implies a slowing of the surface transport during this period.

5. Discussion

[58] A new technique for combining altimeter and Argo data to estimate upper ocean circulation has been presented. The technique makes use of the high temporal and spatial resolution of the altimeter data to remove some of the eddy variability from both hydrographic and subsurface displacement data. Figures 3 and 10 show the reduction in eddy-variability obtained by using the altimeter data. This amounts to a reduction of the noise-to-signal ratio of about 32% in density and 24% in subsurface velocity from float displacements.

[59] The effect of the altimeter data can also be illustrated by comparing estimates of the 1000 db circulation with and without subtraction of the mesoscale eddy variability (Figure 19). In most regions, differences between the two estimates are of order 1 to 2 cm in dynamic height, or 0.5 to 1 cm/s in velocity. Note that the regions with the largest differences are also those with the most eddy variability (see Figure 10). In the estimate of 1000 db dynamic height made using no altimeter data (not shown), boundary currents in both the polar and subtropical gyres appear generally noisier, with more closed or broken contours than the estimate shown in Figure 12. Although use of the altimeter data primarily affects the small-scale features of the time-averaged circulation, it also removes some of the temporal variability in the Gulf Stream, the East and West Greenland Currents and the North Atlantic Current. In the SSH-corrected estimate, these currents range from 2 to 5 cm/s faster at 1000 db and appear as sharper gradients in the estimate of 1000 db dynamic

height. This is the reason for the coherent features visible along the Gulf Stream in Figure 19.

[60] Although the length scales used for the objective maps were carefully modeled to agree with the observed covariances, it is helpful to test the sensitivity of these results to the choice of covariance function. To do so, the velocity estimate along the section studied by *Meinen* [2001] was recomputed using a variety of different values for the short-scale part of the covariance function, l_x . Figure 20 shows the dependence of the maximum velocity and Gulf Stream transport as a function of l_x . Values of l_x ranged from 50 to 150 km in increments of 10 km. For simplicity, values of l_y were also increased in 10 km increments from 30 to 130 km and the short length scales, l_x and l_y , for the subsurface velocity maps and the density maps were held the same. Relaxing these assumptions or allowing the large length scales, L_x and L_y , to vary did not significantly change these results.

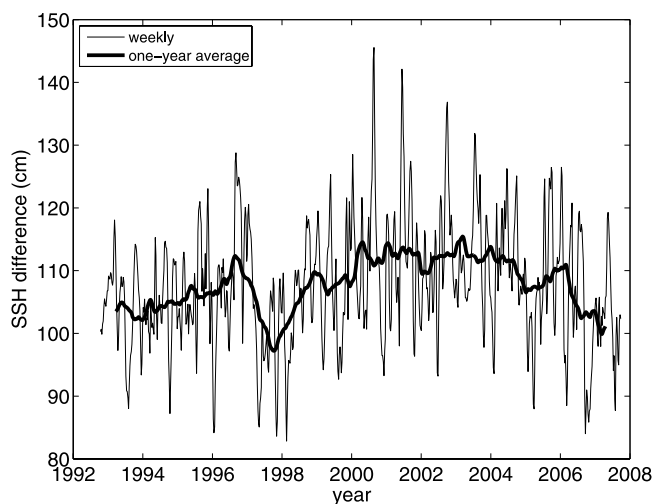


Figure 18. SSH difference across the Gulf Stream along the section studied by *Halkin and Rossby* [1985]. The thin line shows the weekly time series and the thick line shows the one-year running mean. Note the decline in surface transport after 2004.

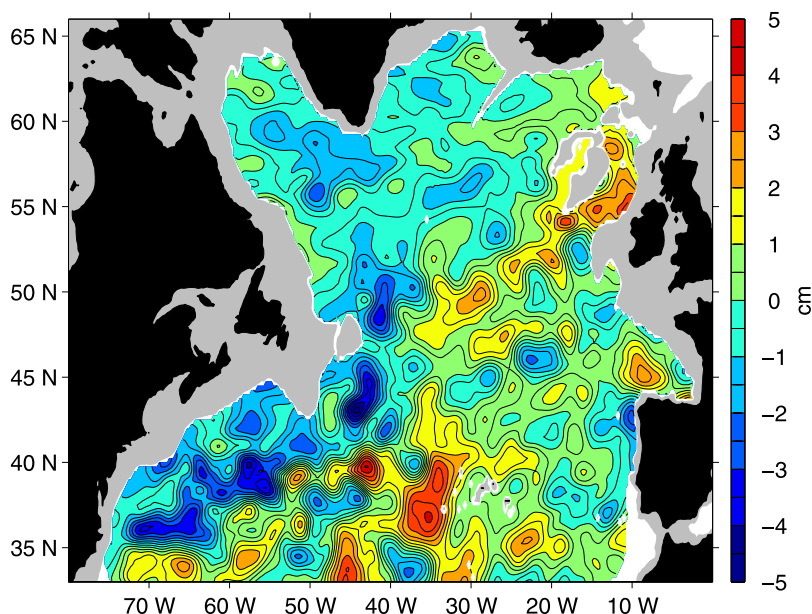


Figure 19. Difference between estimates of 1000 db dynamic height with and without using altimeter data to reduce the eddy noise. Contour interval is 0.5 cm.

[61] Reducing the covariance length scale generally increases the peak surface velocity of the Gulf Stream until the scales become comparable to the $\frac{1}{4}^\circ$ bins used as input to the objective maps; however, the transport begins to fall off for values less than about 90 km. Transport also decreases as scales become too long. However, for the range of scales that provides the best agreement with the covariance functions estimated from the data (approx. 70 to 120 km), transport estimates range from 69 to 70 Sv and maximum velocities range from 39 to 41 cm/s. The relatively narrow range of velocities and transports shown in Figure 20 suggests that these estimates are robust with respect to the choice of parameters in the model covariance function.

[62] The sea-surface height field computed here is based on observations that are largely independent from data used in previous estimates. To investigate agreement between these estimates, Figure 21 shows the difference between our estimate of surface dynamic height and those of Niiler *et al.* [2003], Rio and Hernandez [2004], and Jayne [2006]. In order to avoid introducing real interannual to decadal

variability into these differences, the temporal baseline of each estimate was shifted to the period from 2004 through 2006 using the AVISO maps. For instance, the estimate of Niiler *et al.* [2003] represents a time average over the period from October 1992 through October 2002. For comparison with the present estimate, it was adjusted as follows: $SSH_{Niiler} - SSH_{92-02} + SSH_{04-06}$, where SSH_{Niiler} is the estimate of Niiler *et al.*, and SSH_{92-02} and SSH_{04-06} are averages of the AVISO maps over the periods 1992 through 2002, and 2004 through 2006, respectively.

[63] The best agreement occurs between the present estimate and that of Rio and Hernandez [2004]. The RMS difference between the SSH estimates is 5.1 cm, and the RMS difference in velocity is 6.6 cm/s. Nevertheless, the north-south gradient across the Gulf Stream is significantly larger in the present estimate than that of Rio and Hernandez or any of the other estimates considered. This could reflect a difference in mapping length scales. Rio and Hernandez used scales of 200 km in this region, which is significantly larger than the short scales used here. In addition, Niiler *et al.* [2003] averaged data in $1^\circ \times 1^\circ$

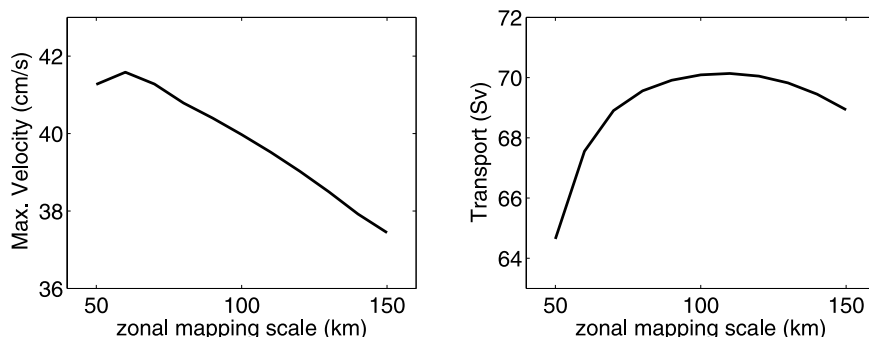


Figure 20. Peak surface velocity and upper 2000 db Gulf Stream transport through the section studied by Meinen [2001] as a function of the zonal scale used in the covariance function.

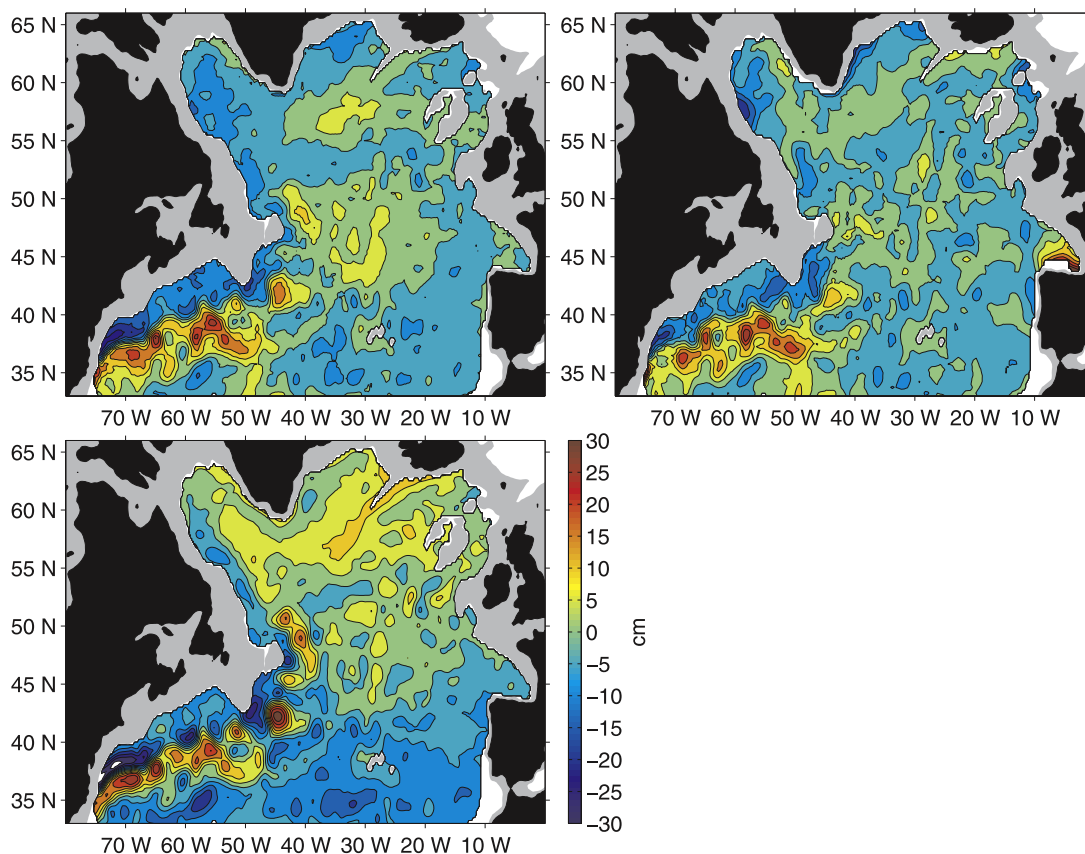


Figure 21. Estimate of surface dynamic height from the present work minus those of *Niiler et al.* [2003, upper left], *Rio and Hernandez* [2004, upper right], and *Jayne* [2006, lower left]. Contour interval is 5 cm.

squares prior to mapping, rather than the $\frac{1}{4}^\circ$ squares used here. This may have filtered out some of the smaller scale variability in that estimate. Further investigation will be required to fully determine the cause of this discrepancy.

[64] The RMS difference between the present estimate and that of *Niiler et al.* [2003] is 5.5 cm (6.6 cm/s in velocity). This is in good agreement with the 4.1 cm error reported for the estimate of *Niiler et al.* [2003] and a median error in the present estimate of 2.5 cm over the study region.

[65] Finally, the estimate of *Jayne* [2006] has an RMS difference of 7.2 cm (8.6 cm/s) with the present estimate. Some of the difference between these two estimates is likely related to the 300 km spatial smoothing that is required to reduce errors in data from the GRACE satellites used by *Jayne*. This is particularly true in the regions with strong spatial gradients such as the Gulf Stream.

[66] If the SSH-corrected Argo data are not used, the RMS difference between the three estimates is 5.5 cm (*Rio05*), 5.8 cm [*Niiler et al.*, 2003], and 7.5 cm [*Jayne*, 2006] for SSH, or 8.0 cm/s, 8.0 cm/s and 9.6 cm/s for surface velocity, respectively.

[67] The technique presented here can be applied to data in most regions across the globe to make robust estimates upper ocean circulation every 2 to 3 years. This will make it possible to estimate large-scale changes in ocean circulation on interannual time scales. As the effects of human induced climate change begin to appear in the ocean's general

circulation, data from satellite altimeters and the Argo array of profiling floats will provide important tools for detecting these signals and understanding the ocean's role in global warming.

[68] **Acknowledgments.** The altimeter products were produced by Ssalto/Duacs and distributed by Aviso with support from CNES. *Rio05* [*Rio and Hernandez*, 2004] was produced by the CLS Space Oceanography Division. The 1992–2002 mean ocean dynamic topography data has been obtained from Nikolai Maximenko (IPRC) and Peter Niiler (SIO). Thanks to S. Jayne for generously providing his estimate of surface dynamic height. Float data were collected and made freely available by Argo (a pilot program of the Global Ocean Observing System) and contributing national programs (<http://www.argo.net/>). This research was carried out at the Jet Propulsion Laboratory, California Institute of Technology, under a contract with the National Aeronautics and Space Administration.

References

- Bretherton, F. P., R. E. Davis, and C. B. Fandry (1976), A technique for objective analysis and design of oceanographic experiments applied to MODE-73, *Deep Sea Res.*, *23*, 559–582.
- Davis, R. E. (1998), Preliminary results from directly measuring middepth circulation in the tropical and South Pacific, *J. Geophys. Res.*, *103*, 24,619–24,639.
- Davis, R. E. (2005), Intermediate-depth circulation of the Indian and South Pacific oceans measured by autonomous floats, *J. Phys. Oceanogr.*, *35*, 683–707.
- Davis, R. E., D. C. Webb, L. A. Regier, and J. Dufour (1992), The Autonomous Lagrangian Circulation Explorer (ALACE), *J. Atmos. Oceanic Technol.*, *9*, 264–285.
- Gilson, J., D. Roemmich, B. Cornuelle, and L.-L. Fu (1998), Relationship of TOPEX/Poseidon altimetric height to steric height and circulation of the North Pacific, *J. Geophys. Res.*, *103*, 27,947–27,965.

- Gouretski, V. V., and K. P. Koltermann (2004), *WOCE Global Hydrographic Climatology* [CD-ROM], Ber. Bundesamt Seeschiffahrt Hydrogr. Rep., 35, 52 pp., Bundesamt Seeschiffahrt Hydrogr., Hamburg, Germany.
- Guinehut, S., P.-Y. Le Traon, and G. Larnicol (2006), What can we learn from global altimetry/hydrography comparisons?, *Geophys. Res. Lett.*, 33, L10604, doi:10.1029/2005GL025551.
- Halkin, D., and H. T. Rossby (1985), The structure and transport of the Gulf Stream at 73°W, *J. Phys. Oceanogr.*, 15, 1439–1452.
- Jayne, S. R. (2006), Circulation of the North Atlantic Ocean from altimetry and the Gravity Recovery and Climate Experiment geoid, *J. Geophys. Res.*, 111, C03005, doi:10.1029/2005JC003128.
- Lavender, K. (2001), The general circulation and open-ocean deep convection in the Labrador Sea: A study using subsurface floats, Ph.D. thesis, pp. 119–120, Univ. of California, San Diego, Calif.
- Lavender, K. L., R. E. Davis, and W. B. Owens (2000), Mid-depth recirculation observed in the interior Labrador and Irminger seas by direct velocity measurements, *Nature*, 407, 66–69.
- Lavender, K. L., W. B. Owens, and R. E. Davis (2005), The mid-depth circulation of the subpolar North Atlantic Ocean as measured by subsurface floats, *Deep Sea Res., Part I*, 52, 767–785.
- Lilly, J. M., P. B. Rhines, F. Schott, K. Lavender, J. Lazier, U. Send, and E. D'Asaro (2003), Observations of the Labrador Sea eddy field, *Prog. Oceanogr.*, 59, 75–176.
- Mann, C. R. (1967), The termination of the Gulf Stream and the beginning of the North Atlantic current, *Deep Sea Res.*, 14, 337–359.
- Meinen, C. S. (2001), Structure of the North Atlantic current in stream—Coordinates and the circulation in the Newfoundland basin, *Deep Sea Res., Part I*, 48, 1553–1580.
- Mercier, H., M. Ollivault, and P.-Y. Le Traon (1993), An inverse model of the North Atlantic general circulation using Lagrangian float data, *J. Phys. Oceanogr.*, 23, 689–715.
- Niiler, P. P., N. A. Maximenko, and J. C. McWilliams (2003), Dynamically balanced absolute sea level of the global ocean derived from near-surface velocity observations, *Geophys. Res. Lett.*, 30(22), 2164, doi:10.1029/2003GL018628.
- Park, J. J., K. Kim, B. A. King, and S. C. Riser (2005), An advanced method to estimate deep currents from profiling floats, *J. Atmos. Oceanic Technol.*, 22, 1294–1304.
- Rio, M.-H., and F. Hernandez (2004), A mean dynamic topography computed over the world ocean from altimetry, in situ measurements and a geoid model, *J. Geophys. Res.*, 109, C12032, doi:10.1029/2003JC002226.
- Roemmich, D., and J. Gilson (2001), Eddy transport of heat and thermocline waters in the North Pacific: A key to understanding interannual/decadal climate variability?, *J. Phys. Oceanogr.*, 31, 675–687.
- Smeed, D. A., and S. G. Alderson (1997), Inference of deep ocean structure from upper-ocean measurements, *J. Atmos. Oceanic Technol.*, 14, 604–615.
- Willis, J. K., D. Roemmich, and B. Cornuelle (2003), Combining altimetric height with broadscale profile data to estimate steric height, heat storage, subsurface temperature, and sea-surface temperature variability, *J. Geophys. Res.*, 108(C9), 3292, doi:10.1029/2002JC001755.
- Willis, J. K., D. Roemmich, and B. Cornuelle (2004), Interannual variability in upper ocean heat content, temperature, and thermocline expansion on global scales, *J. Geophys. Res.*, 109, C12036, doi:10.1029/2003JC002260.
- Willis, J. K., J. M. Lyman, G. C. Johnson, and J. Gilson (2007), Correction to “Recent cooling of the upper ocean”, *Geophys. Res. Lett.*, 34, L16601, doi:10.1029/2007GL030323.
- Willis, J. K., J. M. Lyman, G. C. Johnson, and J. Gilson (2008), In situ data biases and recent ocean heat content variability, *J. Atmos. Oceanic Technol.*, in press.
- Wilson, W. D., W. E. Johns, and S. L. Garzoli (2002), Velocity structure of North Brazil Current rings, *Geophys. Res. Lett.*, 29(8), 1273, doi:10.1029/2001GL013869.
- Zang, X., and C. Wunsch (2001), Spectral description of low-frequency oceanic variability, *J. Phys. Oceanogr.*, 31(10), 3073–3095.

L.-L. Fu and J. K. Willis, Jet Propulsion Laboratory, M/S 300-323, 4800 Oak Grove Drive, Pasadena, CA 91109, USA. (jwillis@caltech.edu)